Geophys. J. Int. (2009) **177,** 104–114 doi: 10.1111/j.1365-246X.2008.04065.x

Elastic wave modelling by an integrated finite difference method

Fiona Hall and Yanghua Wang

Centre for Reservoir Geophysics, Department of Earth Science and Engineering, Imperial College, London SW7 2BP, *UK.*
E-mail: yanghua.wang@imperial.ac.uk

Accepted 2008 November 26. Received 2008 October 20; in original form 2008 April 22

SUMMARY

We have developed a finite difference method for modelling the elastic wave equation in the time domain, based on integrating the elastic parameters. In this method, we adopt the strategy of integrating the elastic parameters over a limited space; so, it is suitable for wave propagation modelling in fractured media, for which we use an equivalent media with the elastic coefficients averaged over a fractured space. This elastic parameters integration allows us to reduce the five simultaneous equations usually used to describe the velocity and stress propagation to just two, in terms of velocity alone, providing a significant saving in computational memory. In this paper, we discuss the derivation and computational implementation of the method for 2-D media, including the seismic source and both reflecting and absorbing boundary conditions, and illustrate it with some synthetic models of heterogeneous, anisotropic and fractured media.

Key words: Numerical solutions; Computational seismology; Wave propagation; Wave scattering and diffraction.

1 INTRODUCTION

In the forward modelling of seismic waveforms, there has been steady improvement in the formulation of finite difference implementations. Explicit second-order time-domain schemes for modelling wave propagation in isotropic homogeneous and heterogeneous cases were proposed by Kelly *et al.* (1976). A second-order staggered grid scheme, based upon the five-equation velocity–stress formulation of the elastic wave equation was proposed by Virieux (1986) to deal with more complicated problems and also to model a boundary between acoustic and elastic media in a stable manner. This was extended to a fourth-order scheme for greater accuracy by Levander (1988). The second-order scheme of Kelly *et al.* (1976) was applied in the frequency domain by Pratt (1990) to allow for more efficient studies of multiple sources and the effects of attenuation.

In this paper, we present a finite difference scheme, based upon the method of integrating elastic parameters over a limited space (Tikhonov & Samarskii 1961). This method works for fully heterogeneous and anisotropic 2-D media. It is implemented using the elastic wave equation written in terms of velocity only, which is an improvement in computational efficiency over the commonly used velocity–stress formulation, because the stress does not need to be calculated or saved. It can be implemented in the time domain, as presented here, or in the frequency domain. In the implementation, we also propose a scheme for how to properly set up a seismic source in the waveform simulation. We illustrate our method by applying it to some synthetic velocity models including heterogeneous, anisotropic and fractured media.

2 FINITE DIFFERENCE SCHEME

The five equations that describe the propagation of seismic waves in a general 2-D elastic medium are

$$\begin{aligned}
\rho\frac{\partial u}{\partial t} &= \frac{\partial \tau_{xx}}{\partial x} + \frac{\partial \tau_{xz}}{\partial z},\\
\rho\frac{\partial w}{\partial t} &= \frac{\partial \tau_{xz}}{\partial x} + \frac{\partial \tau_{zz}}{\partial z},\\
\frac{\partial \tau_{xx}}{\partial t} &= c_{11}\frac{\partial u}{\partial x} + c_{13}\frac{\partial w}{\partial z} + c_{15}\left(\frac{\partial u}{\partial z} + \frac{\partial w}{\partial x}\right),\\
\frac{\partial \tau_{zz}}{\partial t} &= c_{13}\frac{\partial u}{\partial x} + c_{33}\frac{\partial w}{\partial z} + c_{35}\left(\frac{\partial u}{\partial z} + \frac{\partial w}{\partial x}\right),\\
\frac{\partial \tau_{xz}}{\partial t} &= c_{15}\frac{\partial u}{\partial x} + c_{35}\frac{\partial w}{\partial z} + c_{55}\left(\frac{\partial u}{\partial z} + \frac{\partial w}{\partial x}\right),
\end{aligned} \tag{1}$$

where u and w are the particle-velocity components in the horizontal and vertical directions, respectively, τ_{ij} are the (i, j)th components of stress, ρ is density and c_{11}, c_{13}, c_{15}, c_{33}, c_{35}, c_{55} are the six elastic constants relating stress to strain in the 2-D case (Juhlin 1995). The first two equations are derived from Newton's second law and the last three from Hooke's law for an elastic medium. These equations are valid for arbitrary anisotropy and heterogeneity.

To reduce the memory required for forward modelling, we eliminate the stress components and obtain two equations

© 2009 The Authors
Journal compilation © 2009 RAS

$$\begin{aligned}\rho\frac{\partial^2 u}{\partial t^2} &= \left[\frac{\partial}{\partial x}\left(c_{11}\frac{\partial}{\partial x}\right)+\frac{\partial}{\partial x}\left(c_{15}\frac{\partial}{\partial z}\right)+\frac{\partial}{\partial z}\left(c_{15}\frac{\partial}{\partial x}\right)\right.\\ &\quad\left.+\frac{\partial}{\partial z}\left(c_{55}\frac{\partial}{\partial z}\right)\right]u\\ &\quad+\left[\frac{\partial}{\partial x}\left(c_{15}\frac{\partial}{\partial x}\right)+\frac{\partial}{\partial x}\left(c_{13}\frac{\partial}{\partial z}\right)+\frac{\partial}{\partial z}\left(c_{55}\frac{\partial}{\partial x}\right)\right.\\ &\quad\left.+\frac{\partial}{\partial z}\left(c_{35}\frac{\partial}{\partial z}\right)\right]w,\\ \rho\frac{\partial^2 w}{\partial t^2} &= \left[\frac{\partial}{\partial x}\left(c_{15}\frac{\partial}{\partial x}\right)+\frac{\partial}{\partial x}\left(c_{55}\frac{\partial}{\partial z}\right)+\frac{\partial}{\partial z}\left(c_{13}\frac{\partial}{\partial x}\right)\right.\\ &\quad\left.+\frac{\partial}{\partial z}\left(c_{35}\frac{\partial}{\partial z}\right)\right]u\\ &\quad+\left[\frac{\partial}{\partial x}\left(c_{55}\frac{\partial}{\partial x}\right)+\frac{\partial}{\partial x}\left(c_{35}\frac{\partial}{\partial z}\right)+\frac{\partial}{\partial z}\left(c_{35}\frac{\partial}{\partial x}\right)\right.\\ &\quad\left.+\frac{\partial}{\partial z}\left(c_{33}\frac{\partial}{\partial z}\right)\right]w.\end{aligned} \tag{2}$$

This method with two equations uses less memory than the five-equation velocity–stress formulation because there is no need to store the stress components. We model eq. (2) using a finite difference scheme fourth order in space and second order in time, as follows.

Considering the first spatial derivative term of the first equation in (2), let

$$A = \frac{\partial}{\partial x}c_{11}\frac{\partial u}{\partial x}. \tag{3}$$

Following Tikhonov & Samarskii (1961), we define an auxiliary function Q as

$$Q = c_{11}\frac{\partial u}{\partial x} \tag{4}$$

and make a fourth-order finite difference approximation as

$$\frac{\partial}{\partial x}Q(x_i) = \frac{1}{h}\left(-\frac{1}{24}Q_{i+\frac{3}{2}}+\frac{9}{8}Q_{i+\frac{1}{2}}-\frac{9}{8}Q_{i-\frac{1}{2}}+\frac{1}{24}Q_{i-\frac{3}{2}}\right), \tag{5}$$

where h is the distance between the two gridpoints x_i and x_{i+1}.

For the general auxiliary function Q_{i+q}, where $q = \pm\frac{1}{2}$ or $\pm\frac{3}{2}$, we integrate eq. (4) above with respect to x over the interval $[x_{i+q-1/2}, x_{i+q+1/2}]$:

$$\int_{x_{i+q-1/2}}^{x_{i+q+1/2}}\frac{1}{c_{11}}Q\mathrm{d}x = \int_{x_{i+q-1/2}}^{x_{i+q+1/2}}\frac{\partial u}{\partial x}\mathrm{d}x. \tag{6}$$

Making an approximation,

$$Q_{i+q}\int_{x_{i+q-1/2}}^{x_{i+q+1/2}}\frac{1}{c_{11}}\mathrm{d}x = u_{i+q+1/2}-u_{i+q-1/2}, \tag{7}$$

we obtain the following expression for the auxiliary function Q_{i+q}:

$$Q_{i+q} = \left(\int_{x_{i+q-1/2}}^{x_{i+q+1/2}}\frac{1}{c_{11}}\mathrm{d}x\right)^{-1}(u_{i+q+1/2}-u_{i+q-1/2}). \tag{8}$$

Therefore, we have a fourth-order finite difference expression for the spatial derivative (3) as

$$\begin{aligned}A_{i,j} &= \frac{\partial}{\partial x}\left(c_{11}\frac{\partial}{\partial x}\right)u(x_i,z_j,\ell\Delta t)\\ &\approx -\frac{1}{24}a_{i+3/2,j}\left(u^{\ell}_{i+2,j}-u^{\ell}_{i+1,j}\right)+\frac{9}{8}a_{i+1/2,j}\left(u^{\ell}_{i+1,j}-u^{\ell}_{i,j}\right)\\ &\quad-\frac{9}{8}a_{i-1/2,j}\left(u^{\ell}_{i,j}-u^{\ell}_{i-1,j}\right)+\frac{1}{24}a_{i-3/2,j}\left(u^{\ell}_{i-1,j}-u^{\ell}_{i-2,j}\right),\end{aligned} \tag{9}$$

where

$$a_{i+q,j} = \frac{1}{h}\left(\int_{x_{i+q-1/2}}^{x_{i+q+1/2}}\frac{1}{c_{11}(x,z_j)}\mathrm{d}x\right)^{-1}. \tag{10}$$

The situation for a mixed derivative term is slightly different. For example, considering the second term in the first line of eq. (2)

$$B = \frac{\partial}{\partial x}\left(c_{15}\frac{\partial}{\partial z}\right)u, \tag{11}$$

we define the auxiliary function Q as

$$Q = c_{15}\frac{\partial u}{\partial z} \tag{12}$$

and make the fourth-order finite difference approximation to $\partial Q/\partial x$ as in eq. (5). We then integrate eq. (12) with respect to z,

$$\int_{z_{j-1/2}}^{z_{j+1/2}}\frac{1}{c_{15}}Q\mathrm{d}z = \int_{z_{j-1/2}}^{z_{j+1/2}}\frac{\partial u}{\partial z}\mathrm{d}z, \tag{13}$$

and obtain the auxiliary function as

$$Q_{i+q,j} = \left[\int_{z_{j-1/2}}^{z_{j+1/2}}\frac{\mathrm{d}z}{c_{15}(x_{i+q},z)}\right]^{-1}(u_{i+q,j+1/2}-u_{i+q,j-1/2}). \tag{14}$$

Therefore, we have a fourth-order finite difference expression for the spatial derivative (11) as

$$\begin{aligned}B &= \frac{\partial}{\partial x}\left(c_{15}\frac{\partial}{\partial z}\right)u(x_i,z_j,\ell\Delta t)\\ &\approx -\frac{1}{24}b_{i+3/2,j}\left(u^{\ell}_{i+3/2,j+1/2}-u^{\ell}_{i+3/2,j-1/2}\right)\\ &\quad+\frac{9}{8}b_{i+1/2,j}\left(u^{\ell}_{i+1/2,j+1/2}-u^{\ell}_{i+1/2,j-1/2}\right)\\ &\quad-\frac{9}{8}b_{i-1/2,j}\left(u^{\ell}_{i-1/2,j+1/2}-u^{\ell}_{i-1/2,j-1/2}\right)\\ &\quad+\frac{1}{24}b_{i-3/2,j}\left(u^{\ell}_{i-3/2,j+1/2}-u^{\ell}_{i-3/2,j-1/2}\right),\end{aligned} \tag{15}$$

where

$$b_{i+q,j} = \frac{1}{h}\left[\int_{z_{j-1/2}}^{z_{j+1/2}}\frac{1}{c_{15}\left(x_{i+q},z\right)}\mathrm{d}z\right]^{-1}. \tag{16}$$

The time derivatives are modelled using a second-order finite difference method

$$\frac{\partial^2 u(x_i,z_j,t_l)}{\partial t^2} \approx \frac{u^{\ell+1}_{i,j}-2u^{\ell}_{i,j}+u^{\ell-1}_{i,j}}{\Delta t^2}, \tag{17}$$

where at time $\ell = -1$, the particle velocities at all nodes are set to zero.

Finally, the fourth-order finite difference formula for eq. (2) can be presented as

$$u^{\ell+1}_{i,j} = \frac{\Delta t^2}{\rho_{i,j}}(A+B+C+D+E+F+G+H)+2u^{\ell}_{i,j}-u^{\ell-1}_{i,j}, \tag{18}$$

© 2009 The Authors, *GJI*, **177,** 104–114
Journal compilation © 2009 RAS

$$w_{i,j}^{\ell+1} = \frac{\Delta t^2}{\rho_{i,j}}(A' + B' + C' + D' + E' + F' + G' + H') + 2w_{i,j}^{\ell} - w_{i,j}^{\ell-1}, \quad (19)$$

where $A, \cdots H$ and $A', \cdots H'$ are the explicit finite difference expressions, among which A and B are given by (9) and (15), and the rest can be built in exactly the same fashion.

3 IMPLEMENTATION

3.1 Numerical stability

For an isotropic medium, we may use $c_{11} = c_{33} = \lambda + 2\mu$, $c_{55} = \mu$, $c_{13} = \lambda$ and $c_{15} = c_{35} = 0$, where λ and μ are the Lamé parameters related to the P- and S-wave velocities, V_p and V_s, of the isotropic medium. The stability criterion for a finite difference scheme second-order in space and time is (Vireux 1986)

$$\Delta t < \frac{h}{\sqrt{V_p^2 + V_s^2}}, \quad (20)$$

where Δt is the time interval, h is the grid spacing (assumed to be equal in the x and z directions). The use of a fourth-order scheme reduces the stability limit (Levander 1988), and we have found experimentally that our scheme is stable only for Δt less than about 90 per cent of this limit. However, this is still an improvement upon the fourth-order staggered grid method presented in Levander (1988), which was stable for $\Delta t < 0.606\frac{h}{V_p}$.

3.2 Seismic source

The two components of velocity lie within the 2-D plane of the model, and therefore any point source implemented using only these velocity components will always act in a direction within the plane. An example of this is shown in Fig. 1, a snapshot of the horizontal and vertical components, u and w, of particle velocity at time 40 ms. A Ricker source with a dominant frequency of 100 Hz acts in the z direction within a homogeneous material with $V_p = 4200$ m s^{-1}, $V_S = 2700$ m s^{-1} and $\rho = 2490$ kg m^{-3}. The resulting wave has both pressure and shear components. Sometimes this is useful for a particular situation, for example, applying a vertical force at the free surface (Pratt 1990); however, it is often more useful to model an explosive force, which is symmetric about the source location.

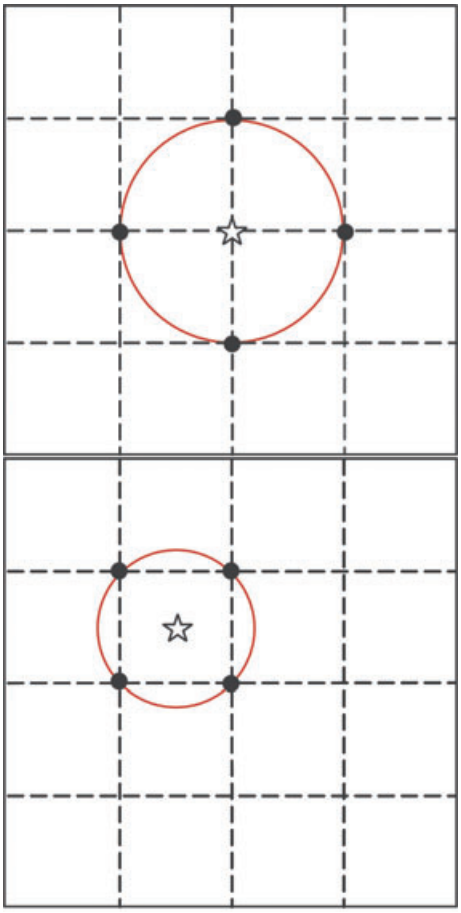


Figure 2. The two different finite difference schemes used to implement the source: (a) a five-point, second-order scheme with the source at the central node; (b) a five-point, second-order scheme with the source in the centre of a cell. The source location is represented by a white star, nodes where the source velocity is calculated by black circles.

The usual method to do this is described in Alterman & Karal (1968). A potential field is introduced, which is inversely

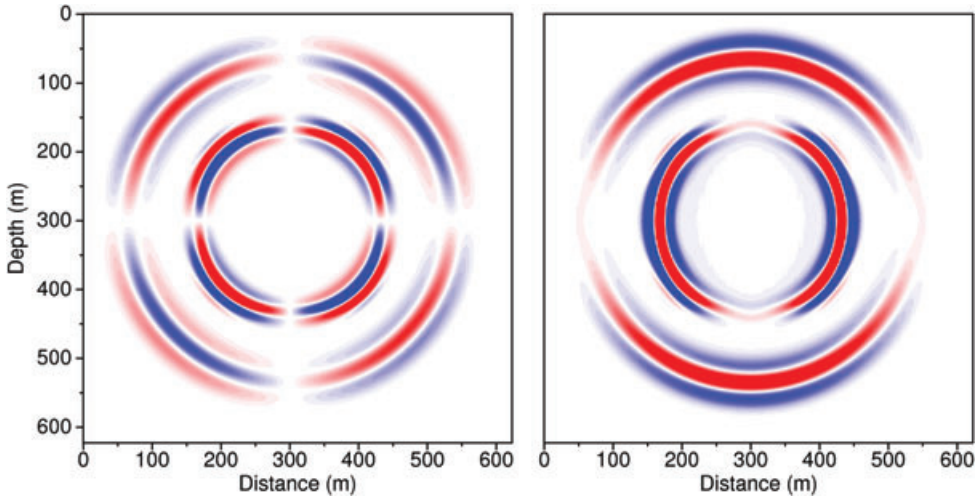


Figure 1. If we simply introduce initial values of u and w at the source location, the resulting wave has both pressure and shear components. These two pictures show snapshots of horizontal and vertical components, u and w, of particle velocity at time 40ms. The source is a Ricker function acting in the z direction.

proportional to the distance from the source. The displacement or velocity field can be found by taking the gradient of the potential. However, at the source location, the potential will have a singularity and will also be large in the area immediately surrounding the source. To address this problem, the area surrounding the source location is required to be homogeneous, then the analytical solution to the elastic wave equation can be computed for this region and appropriate boundary conditions at the edge of this source region to prevent reflections.

This method has been shown to be equivalent to exciting the τ_{xx} and τ_{zz} components of stress at the source location (Virieux 1986). This is a much simpler approach, which we extend to use for our finite difference scheme. To introduce an explosive force, we consider the third and fourth lines in eq. (1). If the source cell is isotropic, these can be written in the form

$$\frac{\partial u}{\partial x} = f\left(\frac{\partial \tau_{xx}}{\partial t}, \frac{\partial \tau_{zz}}{\partial t}\right),$$
$$\frac{\partial w}{\partial x} = f\left(\frac{\partial \tau_{xx}}{\partial t}, \frac{\partial \tau_{zz}}{\partial t}\right). \quad (21)$$

So, for given τ_{xx} and τ_{zz}, u and w can be found using a finite difference approach, combined with the assumption of local symmetry about the source point. We have attempted two different implementations of this finite difference approach, as shown in Fig. 2: (1) a second-order scheme with the source at the central node and (*2*) a second-order scheme with the source in the centre of a cell. In implementing method (1), we must define the velocity at the central, source location as zero for the duration of the source wavelet. This is not required for method (2), as the source point is not on a velocity node. In the situation $\Delta x \neq \Delta z$, method (2) is unchanged; however, a phase shift should be applied for method (1).

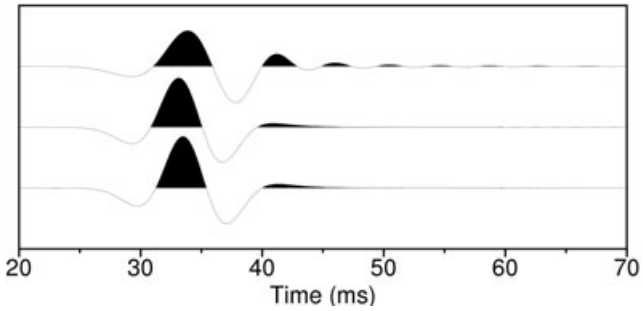


Figure 4. The effect of grid dispersion: modelled seismic traces with (top-panel) two gridpoints per wavelength, (middle-panel) five gridpoints per wavelength and (bottom-panel) ten gridpoints per wavelength. The dominant frequency of the Ricker source is 100Hz and the *S*-wave velocity is 2700ms^{-1}; this gives minimum wavelength of 10.8m. Traces are vertical component traces from a receiver situated 100 m directly below the source.

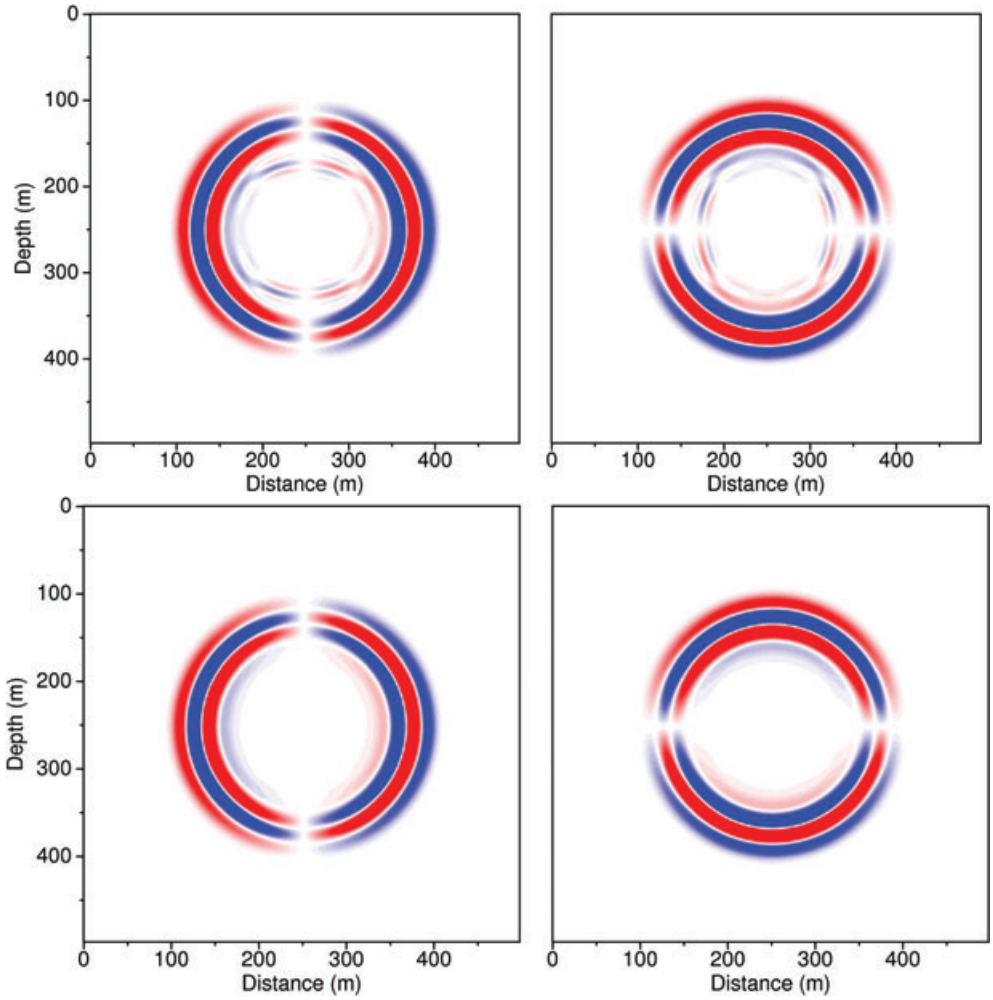


Figure 3. Snapshots showing the horizontal and vertical components of particle velocity after 40 ms, using the two different source implementations shown in Fig. 2. Method (1) (panel a, on the top row) shows numerical artefacts, method (2) (panel b, on the bottom row) does not.

© 2009 The Authors, *GJI*, **177,** 104–114
Journal compilation © 2009 RAS

Fig. 3 compares the results of these methods. The two rows correspond to the two methods respectively, and the two columns are the horizontal and vertical components, respectively, of the particle velocity. The source is a Ricker wavelet with dominant frequency 100 Hz. Material and modelling parameters are the same as for Fig. 1. Method (1) (Fig. 3a) shows numerical artefacts, but method (2) (Fig. 3b) shows the desired circularly symmetric wave front. For method (1), the numerical dispersion and source-generated noises

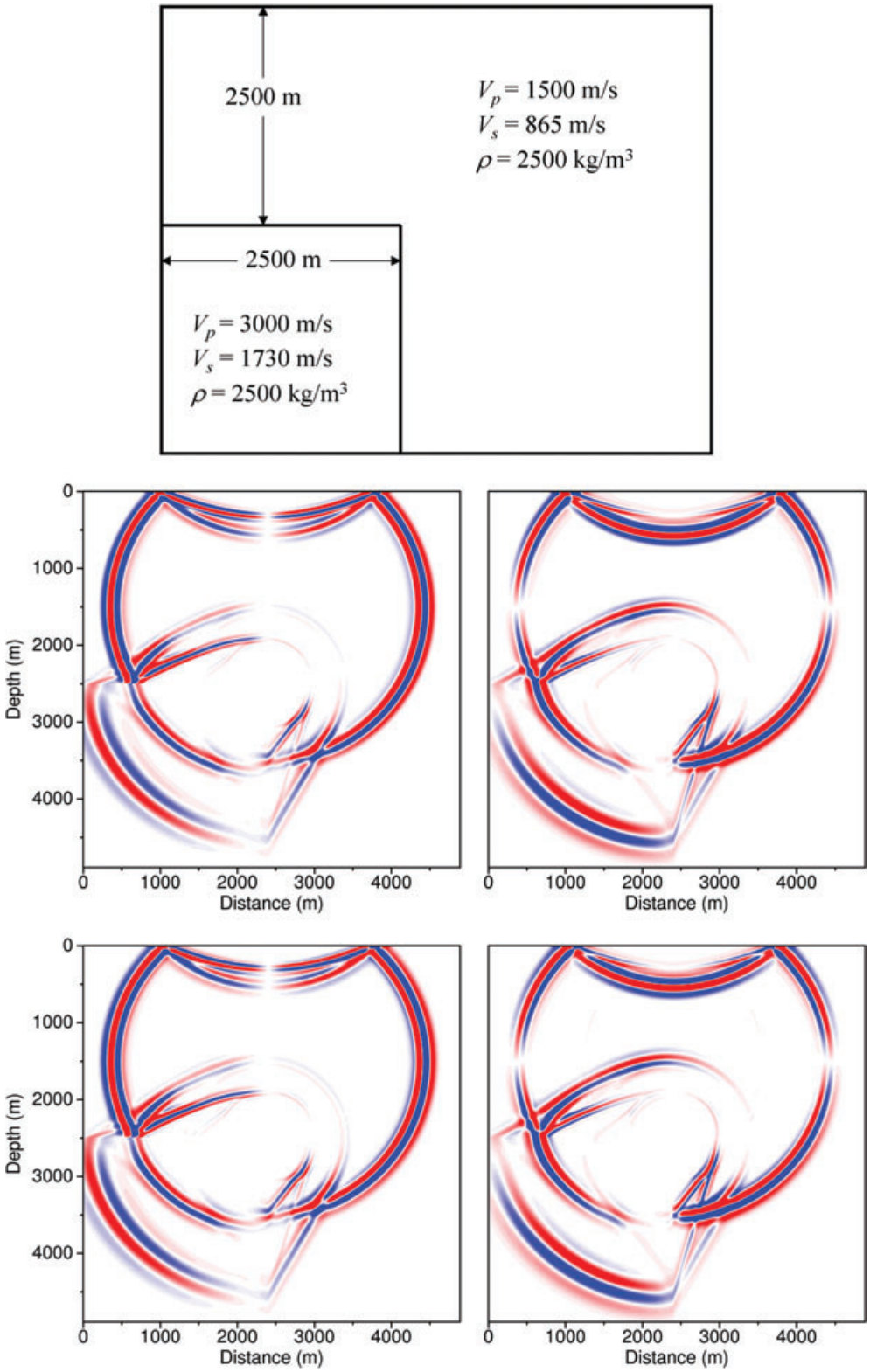


Figure 5. Corner model configuration (top row) horizontal and vertical components after time 1.5s for the velocity–stress staggered grid method (middle row) and our method (bottom row). The source is at (2500, 1500) m.

caused by the discretizing the wave equations with too-coarse grids in the finite difference implementation can be suppressed by using some damage-control techniques such as a flux-corrected transport technique (Yang *et al*. 2002) or a nearly analytical discrete method (Yang *et al*. 2007). But in this paper, we simply chose method (2) for all future implementations.

As the source, we use a Ricker wavelet, where particle velocity varies with time according to

$$u = \pm 2\alpha t \mathrm{e}^{-\alpha t^2}, \tag{22}$$

where α is a constant controlling the frequency bandwidth of the wavelet. A fourth-order finite difference method usually requires

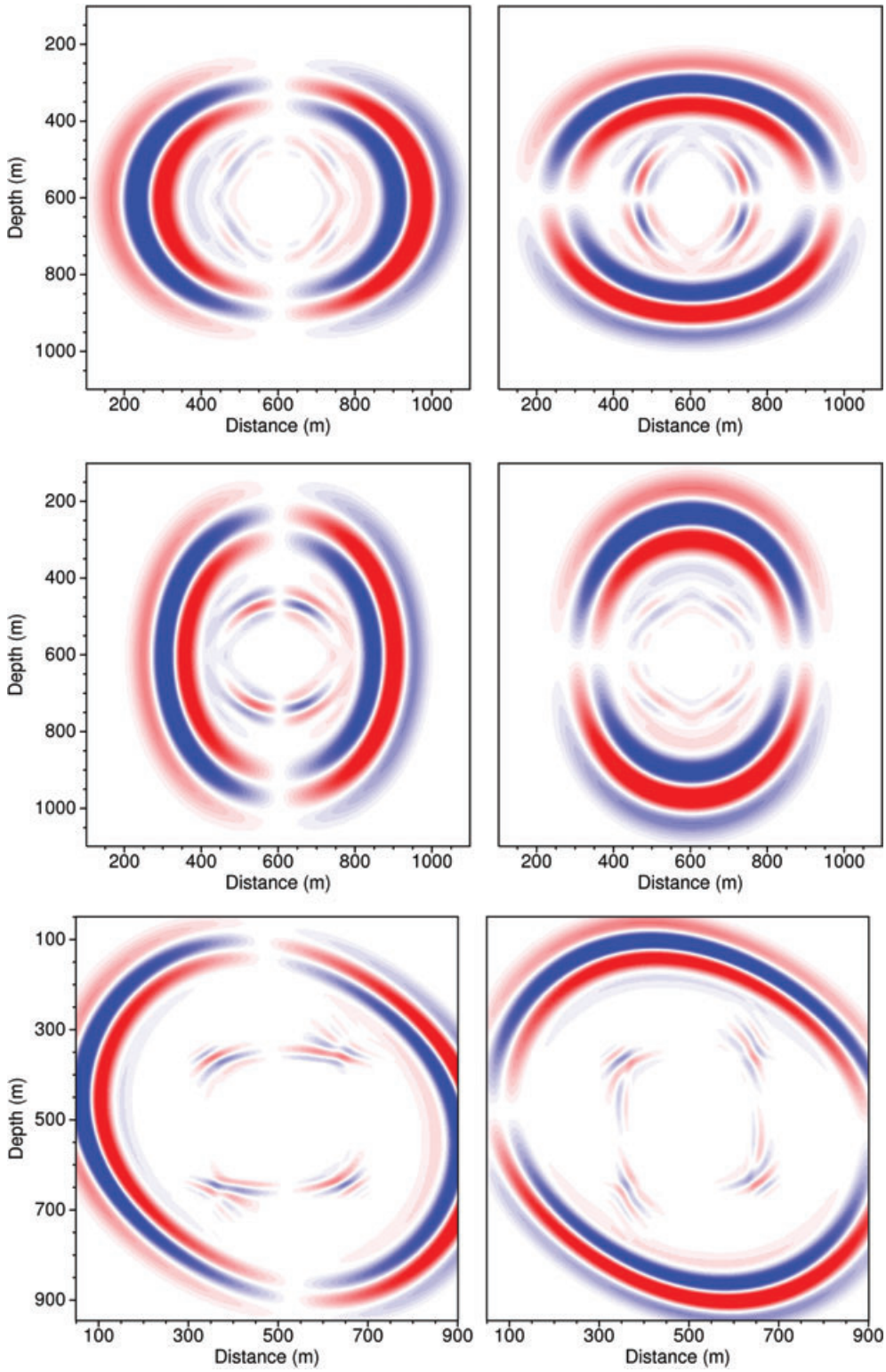


Figure 6. Homogeneous media with anisotropy. Source is at (600, 600) m for the top and middle and at (500, 500) m for the bottom. Time slices shown after 150 (top and middle) and 160 ms (bottom).

© 2009 The Authors, *GJI*, **177,** 104–114
Journal compilation © 2009 RAS

five gridpoints per wavelength to avoid grid dispersion; simple tests in Fig. 4 demonstrate that the same is true for our method.

3.3 Boundary conditions

Reflections from the sides and bottom of the model are generally undesirable and need to be suppressed. We do this using a numerical sponge (Cerjan *et al.* 1985), a zone at the edge of the model where the velocity amplitude of each node is artificially reduced by multiplying with a factor, G, which is equal to one at the inner boundary of the sponge and decreases towards the outer boundary. The effectiveness of this method relies upon the choice of the multiplier G, we found that the function used in Cerjan *et al.* (1985), where for example of the left-hand boundary the velocity of each node, with index i, is multiplied by a factor

$$G = \mathrm{e}^{-[0.015(10-i)]^2}, \tag{23}$$

and a spongewidth of 10 nodes was suitable to suppress reflections to a satisfactory level.

At the top surface of the model, which generally represents the Earth's surface, absorbing boundary conditions are not usually physically realistic, as we wish to allow reflections and surface waves. We therefore use a free surface boundary condition, where the normal stresses are fixed at zero. We implement this by introducing two extra rows of fictional gridpoints above the free surface and using appropriate symmetry conditions, in the manner of Kelly *et al.* (1976).

4 HETEROGENEOUS, ANISOTROPIC AND FRACTURED MODELS

At no point in our formulation of the finite difference scheme do we assume that density or seismic velocity are homogeneous, therefore boundary conditions between layers are implicitly met; and it is simple to implement the scheme under heterogeneous conditions, the only consideration being that the source must be in a locally homogeneous finite difference cell.

We illustrate our method by applying it to some simple synthetic velocity models. The first test we conduct is for the corner model case (Fig. 5), where we can see refracted, reflected and diffracted waves. The corner model is a stringent test of a finite difference method (Virieux 1986) and has been shown to produce discrepancies

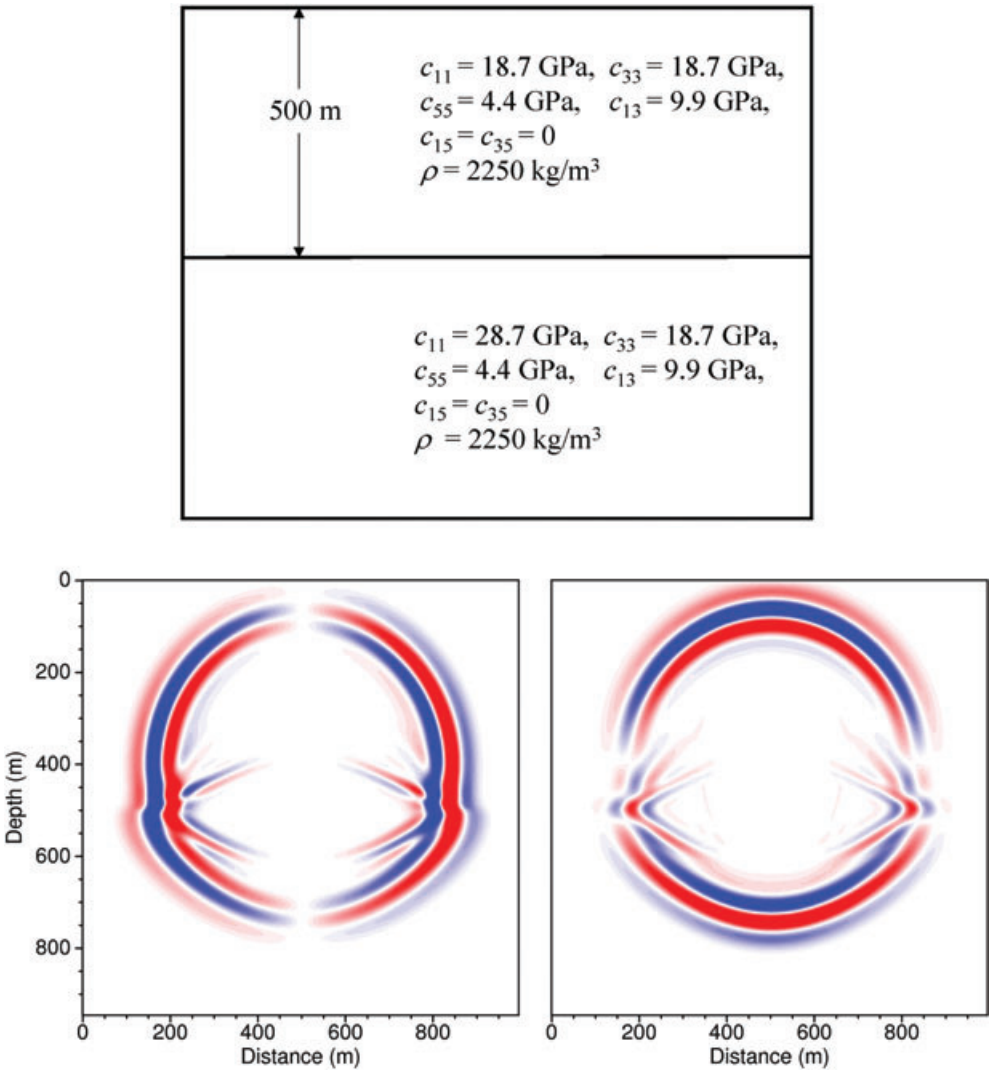


Figure 7. Two-layer isotropic/anisotropic model configuration (top), horizontal and vertical velocity time slices after 150 ms (middle and bottom). The source is at (500, 400) m.

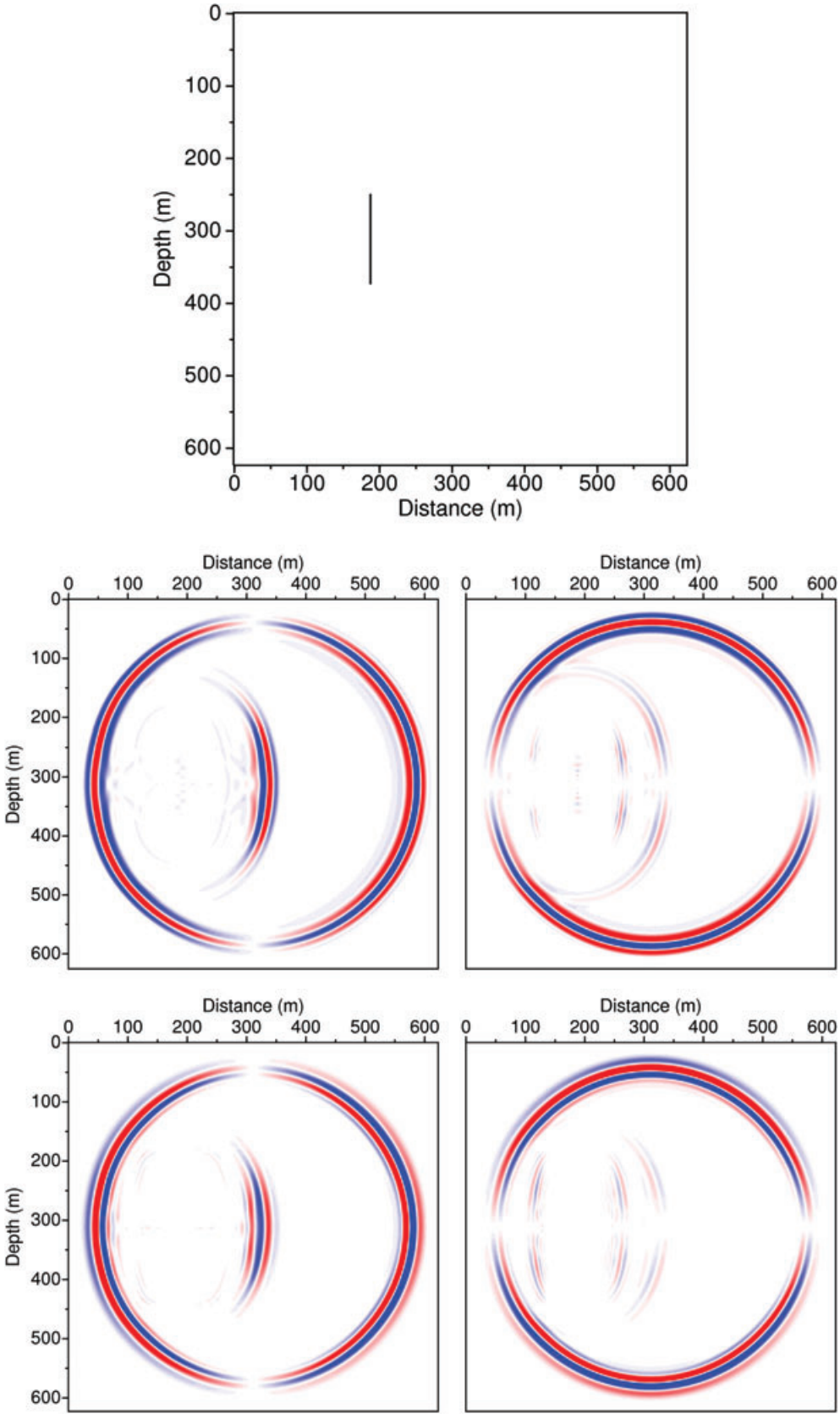


Figure 8. Single fracture model. The fracture location (top), horizontal and vertical components after time 0.1 s using the velocity–stress staggered grid method (middle) and our method (bottom).

© 2009 The Authors, *GJI*, **177,** 104–114
Journal compilation © 2009 RAS

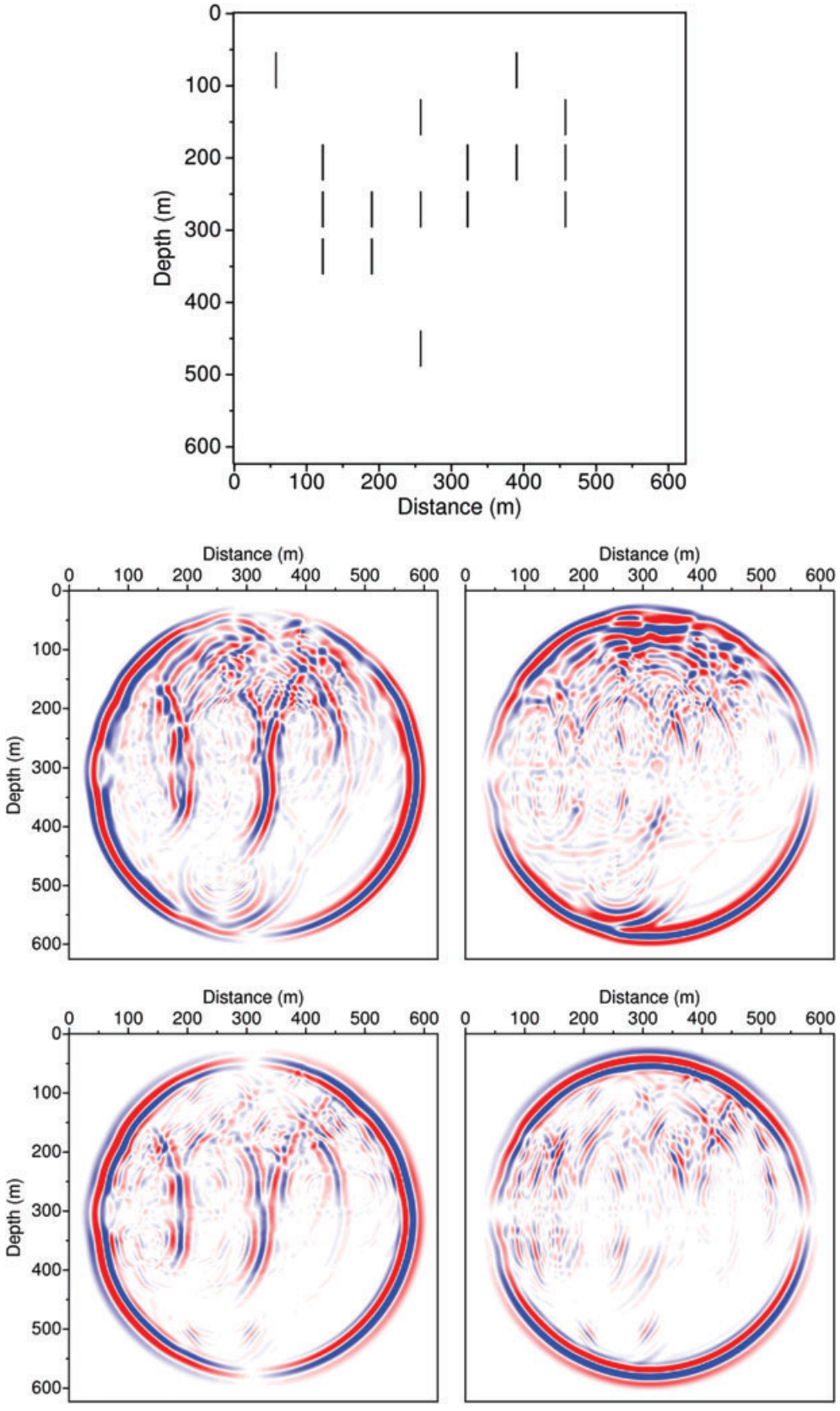


Figure 9. Multiple aligned fracture model. The fracture locations (top), horizontal and vertical components after time 0.1 s using the velocity–stress staggered grid method (middle) and our method (bottom).

between the results of homogeneous and heterogeneous formulations (Kelly *et al.* 1976). We show that the results of our test are essentially the same to the results from the conventional fourth-order velocity–stress staggered grid method (Levander 1988). The slight discrepancy in wave shapes is due to the difference in source signatures because the conventional method needs a stress source, and our method uses a velocity source.

Fig. 6 shows propagation in different anisotropic media. The model parameters are taken from Juhlin (1995). The elastic parameters for three anisotropic models are as follows:

Top row, $c_{11} = 28.9$, $c_{33} = 18.9$, $c_{55} = 4.4$, $c_{13} = 16$, $c_{15} = c_{35} = 0$ (GPa).

Middle row: $c_{11} = 18.9$, $c_{33} = 28.9$, $c_{55} = 4.4$, $c_{13} = 16$, $c_{15} = c_{35} = 0$ (GPa).

Bottom row: $c_{11} = 26.6$, $c_{33} = 21.8$, $c_{55} = 3.9$, $c_{13} = 15.7$, $c_{15} = 1.8$, $c_{35} = 2.3$ (GPa).

Density in all models is 2250 kg m^{-3}. Time slices shown after 150 ms (top and middle) and 160 ms (bottom). We can see the different velocities in fast and slow directions. The fast direction does not need to be aligned with the finite difference grid, it can lie in any arbitrary orientation, as in the third example. Because of the anisotropy, we also see the generation of *S* waves behind the wavefront of *P* waves.

In Fig. 7, we test the method for an isotropic/anisotropic two-layer model and find that it produces stable results. We can see the expected refracted, reflected and converted waves from the interface at 500 m depth, while the point source is at a depth of 400 m, just above the interface.

To show the advantages of this new method, we also look at the field from a model containing fractures. To include the fractures, we use the equivalent medium method (Coates & Schoenberg 1995, Igel *et al*. 1997, Liu *et al.* 2000, Wu *et al.* 2005), where the elastic parameters of cells that are intersected by the fracture are replaced by those of an equivalent anisotropic medium. An advantage of this method is that it does not require a special treatment of the displacement-discontinuity conditions on the fractures (Saenger & Shapiro 2002, Vlastos *et al*. 2003, Saenger *et al*. 2004). In contrast, the popular linear-slip model (Schoenberg 1980) needs explicit displacement-discontinuity treatment (Zhang 2005). Wu *et al*. (2005) compared the effect of the equivalent medium method and linear-slip model on open fluid-filled fracture model. The fractures are tapered hyperbolically, as in Vlastos *et al.* (2003).

Fig. 8 shows an example of a model with a single dry fracture (Liu *et al.* 2000). The Background *P*- and *S*-wave velocities are 3000 and 1700 m s^{-1}, and density is 2300 kg m^{-3}. The source is a Ricker wavelet of peak frequency 100 Hz at (312.5, 312.5) m. The fracture length is 125 m, in contrast to the cell size of 2.5 m. The wavefield (Fig. 8) from an individual fracture shows few differences between our method and the conventional staggered grid finite difference method (Levander 1988), except that diffractions from the fracture tips are slightly reduced. Krüger e*t al*. (2005) discussed the scattering and diffraction by a single crack with staggered grid finite difference method.

However, as shown in Fig. 9, if we consider the field from a randomly distributed set of aligned fractures, we can see that the overall effect is increased. The fractures in Fig. 9 are the same dry fractures as that in Fig. 8, with a shorter fracture length of 50 m (to fit them in the model). All the elastic parameters are the same. In the conventional method, the diffractions generated from the fracture tips are stronger, and their interference with each other result in a much more complicated wavefield than that modelled using the method presented in this paper. Orlowsky *et al*. (2003) analysed the effect of parallel crack distribution using the staggered grid method.

5 CONCLUSIONS

We have developed a finite difference scheme for elastic wave-equation forward modelling, based on integrating the elastic parameters. The method with two equations uses less memory than the five-equation velocity–stress formulation. The integration technique replaces point scatters with averaged elastic parameters and has potential for reducing diffractions from scatterers such as fracture tips. In the implementation, we also propose a scheme to properly set up the seismic source in the wave field simulation. This method is applicable to seismic wavefield simulation in heterogeneous, anisotropic and fractured 2-D media.

ACKNOWLEDGMENTS

We are grateful to the sponsors of the Centre for Reservoir Geophysics, Imperial College London, for supporting this research. We also thank Dr Y. Rao for providing her code of the velocity–stress staggered grid method for generating parts of Figs 5, 8 and 9.

REFERENCES

Alterman, Z. & Karal, F.C., 1968. Propogation of elastic waves in layered media by finite difference methods, *Bull. seism. Soc. Am.,* **58,** 367–398.

Cerjan, C., Kosloff, D., Kosloff, R. & Reshef, M., 1985. A non-reflecting boundary condition for discrete acoustic-wave and elastic-wave equations, *Geophysics,* **50,** 705–708.

Coates, R. T. & Schoenberg, M., 1995. Finite-difference modelling of faults and fractures, *Geophysics,* **60,** 1514–1526.

Igel, H., Ben-Zion, Y. & Leary, P.C., 1997. Simulation of *SH*- and *P-SV*-wave propagation in fault zones, *Geophys. J. Int.,* **128,** 533–546.

Kelly, K.R., Ward, R.W., Treitel, S. & Alford, R.M., 1976. Synthetic seismograms: a finite difference approach, *Geophysics,* **41,** 2–27.

Krüger, O.S., Saenger, E.H. & Shapiro, S.A., 2005. Scattering and diffraction by a single crack: an accuracy analysis of the rotated staggered grid, *Geophys. J. Int.,* **162,** 25–31.

Juhlin, C., 1995. Finite-difference elastic wave propagation in 2D heterogeneous transversely isotropic media, *Geophys. Prospect.,* **43,** 843–858.

Levander, A.R., 1988. Fourth-order finite-difference *P-SV* seismograms, *Geophysics,* **53,** 1425–1436.

Liu, E., Hudson, J.A. & Pointer, T.A., 2000. Equivalent medium representation of fractured rock, *J. geophys. Res.,* **105,** 2981–3000.

Orlowsky, B., Saenger, E.H., Guéguen, Y. & Shapiro, S.A., 2003. Effects of parallel crack distributions on effective elastic properties: a numerical study, *Int. J. Fract.,* **124,** L171–L178.

Pratt, R.G., 1990. Frequency-domain elastic wave modelling by finite-differences: a tool for crosshole seismic imaging, *Geophysics,* **55,** 626–632.

Saenger, E.H. & Shapiro, S.A., 2002. Effective velocities in fractured media: a numerical study using the rotated staggered grid, *Geophys. Prospect.,* **50,** 183–194.

Saenger, E.H., Krüger, O.S. & Shapiro, S.A., 2004. Effective elastic properties of randomly fractured soils: 3D numerical experiments, *Geophys. Prospect.,* **52,** 183–195.

Schoenberg, M., 1980. Elastic wave behaviour across linear slip interfaces, *J. acoust. Soc. Am.,* **68,** 1516–1521.

Tikhonov, A. & Samarskii, A., 1961. Homogeneous difference schemes, *Z. Vycisl. Mat. i Mat. Fiz.,* **1,** 5–63.

© 2009 The Authors, *GJI*, **177,** 104–114
Journal compilation © 2009 RAS

Virieux, J., 1986. *P-SV* wave propagation in heterogeneous media: velocity-stress finite-difference method, *Geophysics,* **51,** 889–901.

Vlastos, S., Liu, E., Main, I.G. & Li, X.-Y., 2003. Numerical simulation of wave propagation in media with discrete distributions of fractures: effects of fracture sizes and spatial distributions, *Geophys. J. Int.,* **152,** 649–668.

Wu, C.L., Harris, J.M., Nihei, K.T. & Nakagawa, S., 2005. Two-dimensional finite-difference seismic modeling of an open fluid-filled fracture: comparison of thin-layer and linear-slip models, *Geophysics,* **70,** T57–T62.

Yang, D.H., Liu, E., Zhang, Z.J. & Teng, J., 2002. Finite-difference modelling in two-dimensional anisotropic media using a flux-corrected transport technique, *Geophys. J. Int.,* **148,** 320–328.

Yang, D.H., Song, G.J., Chen, S. & Hou, B.Y., 2007. An improved nearly analytical discrete method: an efficient tool to simulate the seismic response of 2-D porous structures, *J. geophys. Eng.,* **4,** 40–52.

Zhang, J.F., 2005. Elastic wave modelling in fractured media with an explicit approach, *Geophysics,* **70,** T75–85.